APC mutations lead to cytokinetic failures in vitro and tetraploid genotypes in *Min* mice

Christine M. Caldwell, Rebecca A. Green, and Kenneth B. Kaplan

Section of Molecular and Cell Biology, University of California, Davis, Davis, CA 95616

Previous research has proposed that genomic instability contributes to cancer progression, with its initiation linked to tetraploid cell formation (Duesberg, P., and R. Li. 2003. *Cell Cycle.* 2:202–210; Ganem, N.J., Z. Storchova, and D. Pellman. 2007. *Curr. Opin. Genet. Dev.* 17:157–162). However, there is little direct evidence linking cancer-causing mutations with such events, and it remains controversial whether genomic instability is a cause or an effect of cancer. In this study, we show that adenomatous polyposis coli (APC) mutations found in human colorectal cancers dominantly inhibit cytokinesis by preventing mitotic spindle anchoring at the anaphase cortex and, thus, blocking initiation of the cytokinetic furrow. We find that dividing crypt cells in the small intestines of $APC^{Min/+}$ mice exhibit similar mitotic defects, including misoriented spindles and misaligned chromosomes. These defects are observed in normal crypt cells with wild-type levels of β-catenin and, importantly, are associated with tetraploid genotypes. We provide direct evidence that the dominant activity of APC mutants induces aneuploidy in vivo. Our data support a model whereby tetraploid cells represent a first step in the onset of genomic instability and colorectal cancer.

Introduction

To explain how genomic instability arises in cancer cells, one model posits that the formation of cells with tetraploid genomes represents a transient initiating event (see model in Fig. 7; Duesberg and Li, 2003; Ganem et al., 2007). Consistent with this model, it has recently been observed that tetraploid genomes promote an increase in numerical and structural chromosomal aberrations in p53-deficient cells (Storchova and Pellman, 2004; Fujiwara et al., 2005; Storchova et al., 2006). Although the precise mechanisms that lead to the chromosomal defects in these cells are unclear, the stress of maintaining tetraploid genomes may select for viable resolutions that give rise to a variety of genomic configurations. Such an increase in genomic instability would allow nascent tumor cells to sample a wide genetic space, increasing their chance of finding a genomic configuration to overcome their normal growth constraints. If tetraploid genomes play an initiating role in genomic instability in cancer, it is predicted that cancer-promoting lesions will result in the early appearance of tetraploid cells in sufficient numbers to ensure the selection of genetic winners. In this study, we provide evidence that dominant mutations in the tumor suppressor gene *adenomatous polyposis coli* (*APC*), which is frequently observed in human colorectal cancer, drive tetraploid formation by causing failures in cytokinesis before the earliest steps associated with colorectal cancer progression.

Previous work has implicated APC in the regulation of mitotic events, including formation of the mitotic spindle and proper functioning of the spindle checkpoint (Green and Kaplan, 2003; Tighe et al., 2004; Green et al., 2005; Draviam et al., 2006). APC associates with the mitotic spindle through its interaction with microtubules and with the microtubule plus end–binding protein EB1 (Munemitsu et al., 1994; Smith et al., 1994; Su et al., 1995; Morrison et al., 1998; Green et al., 2005). In previous work, we have shown that APC mutations similar to those found in human cancer patients act dominantly to prevent the interaction of APC with EB1 and, thus, inhibit microtubule dynamics and proper chromosome alignment (Green et al., 2005). Although microtubule dynamics are important for chromosome alignment during metaphase, mitotic spindle defects can also interfere with cytokinesis in tumor cells (Wheatley and Wang, 1996; Alsop and Zhang, 2003; Pihan et al., 2003; Wang et al., 2004). In part, this reflects the role of multiple sets of microtubules in regulating initiation and ingression of the cleavage furrow; peripheral overlapping microtubules at the equatorial cortex converge to initiate furrow formation, whereas

Correspondence to Kenneth B. Kaplan: kbkaplan@ucdavis.edu

R.A. Green's present address is Ludwig Institute for Cancer Research, La Jolla, CA 92093.

Abbreviations used in this paper: APC, adenomatous polyposis coli; EYFP, enhanced YFP.

The online version of this article contains supplemental material.

© The Rockefeller University Press $30.00
The Journal of Cell Biology, Vol. 178, No. 7, September 24, 2007 1109–1120
http://www.jcb.org/cgi/doi/10.1083/jcb.200703186

the spindle midzone is critical for completing furrow ingression (Rappaport, 1961; Glotzer, 2001; Saint and Somers, 2003; Inoue et al., 2004; D'Avino et al., 2005). The ability of APC mutants to dominantly interfere with mitotic spindle assembly led us to ask whether a single APC allele might induce failures in cytokinesis that contribute to genomic instability and cancer progression.

Results

APC$^{1-1,450}$ inhibits cytokinesis

To address the possibility that APC mutants compromise cytokinesis, we examined the long-term effect of expressing the dominant-negative APC$^{1–1,450}$ (amino acids 1–1,450) mutant on chromosomal ploidy. This allele is representative of *APC* mutations observed in human colorectal cancer (Lamlum et al., 1999; Sieber et al., 2000; Fearnhead et al., 2001). We created HEK-293 cell lines stably expressing APC$^{1–1,450}$ under an ecdysone-inducible promoter and control cells lacking the hormone receptor required for expression (labeled as the control in figures; Green and Kaplan, 2003). Immunoblotting for the tagged APC allele showed relatively constant expression similar to endogenous levels over the course of the experiment (Green and Kaplan, 2003; Green et al., 2005; and unpublished data). In control cells, we observed a constant and very low incidence of binucleate cells (1–2%) and few multinucleated (more than two nuclei) cells over 10 d (Fig. 1, A and B, control). In contrast, cells expressing APC$^{1–1,450}$ exhibited a steady increase in the numbers of both binucleate and multinucleate cells during the course of the experiment (Fig. 1, A [binucleate and multinucleate] and B), with each category reaching 10% of the total cell population. Multiple stable cell lines all exhibited the same trend: after >3 d of APC$^{1–1,450}$ expression, we observed a mean of 10.26% binucleate (SD = 6.34%) and 8.34% multinucleate (SD = 5.27%) compared with control cells with 0.63% bincucleate (SD = 0.37%) and 0.33% multinucleate (SD = 0.1%). These results are

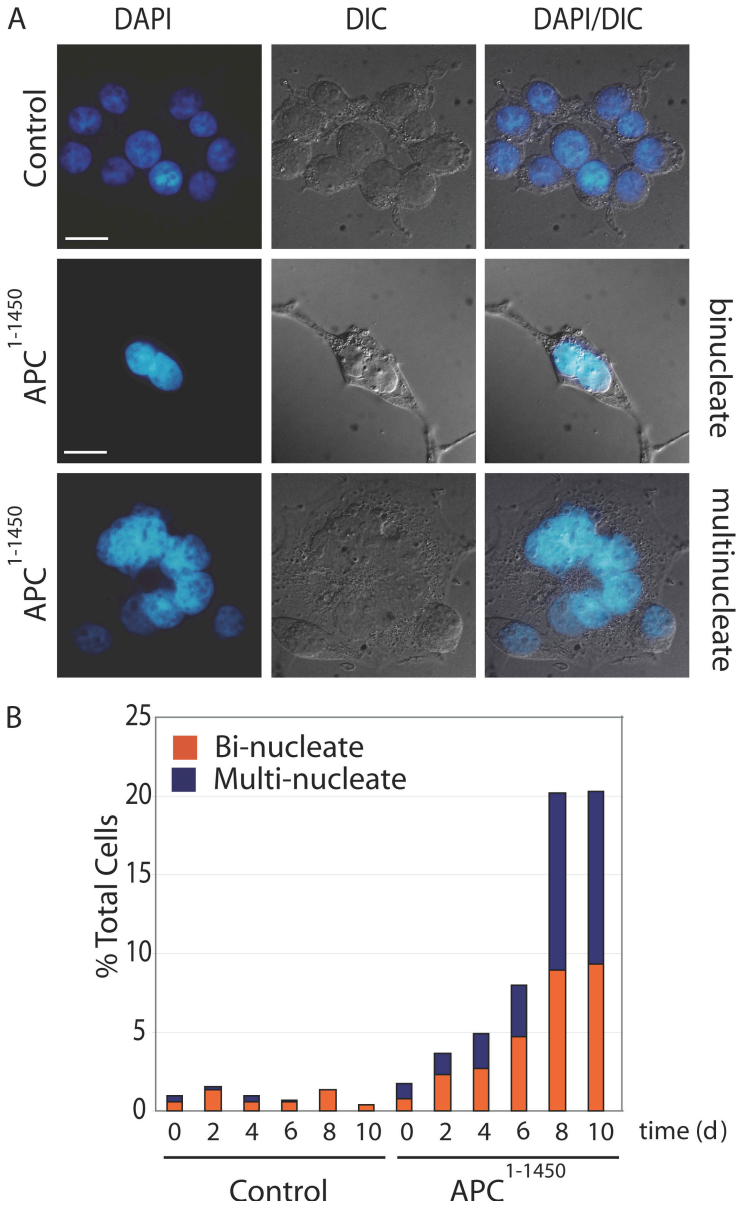

Figure 1. **Expression of APC$^{1–1,450}$ results in the accumulation of binucleate and multinucleate cells.** (A) Cells were fixed and stained with DAPI to visualize normal, binucleate, and multinucleate cells. (B) The percentage of control cells or cells expressing APC$^{1–1,450}$ with more than one nuclei were determined after fixing and staining cells to visualize chromosomes 0, 2, 4, 6, 8, and 10 d after induction. The percentage of cells that were binucleate (orange) or multinucleate (purple) were calculated for a minimum of 300 cells. The data presented are representative of three separate experiments performed at different time intervals. The range of multinucleated cells observed for all experiments is presented in Table I. DIC, differential interference contrast. Bars, 10 μm.

consistent with previous findings that cells expressing similar APC mutants become polyploid over time (Fodde et al., 2001; Tighe et al., 2004).

To examine the possibility that $APC^{1–1,450}$ expression gives rise to polyploid cells as a result of failed cytokinesis, we monitored the behavior of chromosomes in time-lapse videos using an E-YFP-histone 2B (H2B) fusion. Cells with chromosomes aligned in metaphase were identified and filmed as they proceeded through anaphase (Fig. 2 and Video 1, available at http://www.jcb.org/cgi/content/full/jcb.200703186/DC1). After chromosome segregation in control cells, cytokinetic ingression was observed in brightfield images (Fig. 2 B, 18 min; arrow). Control cells initiated a furrow, completed cytokinesis, and returned to their interphase state ~30 min after anaphase began. In many cells expressing $APC^{1–1,450}$, we observed no evidence of furrow initiation after anaphase (Fig. 2, C and D; and Video 2), and chromosomes became tightly juxtaposed 10 min after segregation, which is consistent with a collapse of the anaphase spindle (Fig. 2 C, 28 min). Chromosomes began to decondense, and nuclei formed close to one another as cells returned to their interphase state. We believe that this behavior gives rise to the binucleate (i.e., polyploid) cells we observed in Fig. 1 A. Consistent with cytokinetic failure, staining of cells with antibodies against γ-tubulin revealed binucleate and multinucleate interphase cells with two or more centrosomes (unpublished data). We conclude that the expression of $APC^{1–1,450}$ results in binucleated cells as a result of failures to carry out cytokinesis before exiting mitosis.

We suspected that defects in spindle microtubules were responsible for the failed cytokinesis in cells expressing $APC^{1–1,450}$ for at least two reasons. First, an allelic series of APC mutants with increasingly severe defects in mitotic spindle organization correlated with the number of bi- and multinucleated cells (Fig. S1 A, available at http://www.jcb.org/cgi/content/full/jcb.200703186/DC1; and not depicted; Green et al., 2005). The appearance of bi- and multinucleated cells is also increased in colorectal tumor cell lines with truncating mutations in APC (Fig. S1 A, SW480). Second, we observed that compared with control cells, large regions of the cortex of cells expressing $APC^{1–1,450}$ lack growing microtubule plus ends marked with EB1-GFP, and these spindles undergo increased rotations with respect to the spindle axis (Fig. 3, A–C; arrows; and compare Video 4 with Video 3).

Failed spindle anchoring blocks cytokinesis

As furrow initiation is specified by the mitotic spindle, we were particularly intrigued by the observation that microtubules make less contact with the cell cortex, and spindles appear to undergo considerable rotation when EB1-GFP was monitored in cells expressing $APC^{1–1,450}$ (Video 4). We reasoned that the rotation of anaphase spindles may impact the ability of cells to initiate a cytokinetic furrow. To test this possibility, we compared the behavior of the mitotic apparatus with respect to the onset of anaphase and furrow initiation in control cells with cells expressing $APC^{1–1,450}$. Metaphase cells expressing GFP fusions to tubulin,

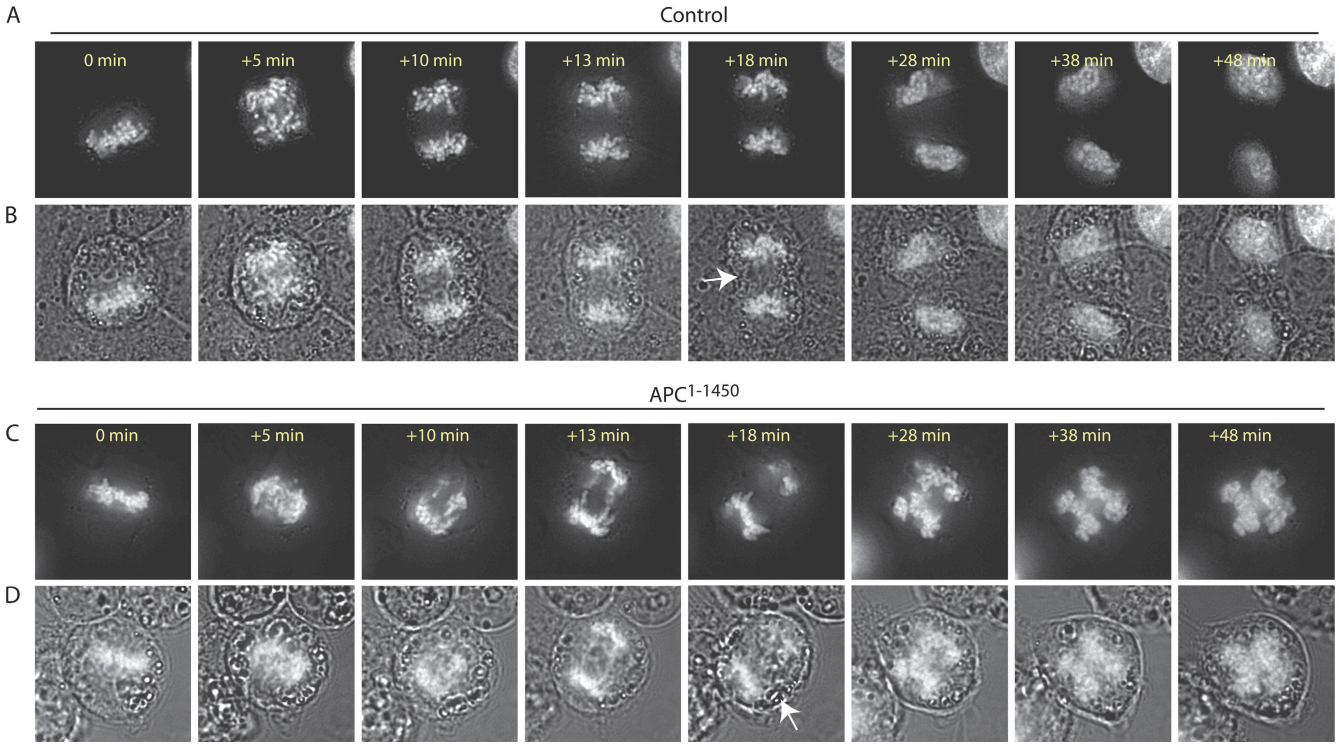

Figure 2. **Expression of $APC^{1–1,450}$ results in cytokinetic failure.** (A–D) EYFP–H2B was transiently expressed in the indicated cell lines. Metaphase cells were filmed, and select time points from videos (Videos 1 and 2, available at http://www.jcb.org/cgi/content/full/jcb.200703186/DC1) were formatted to show fluorescence (A and C) or the fluorescence images overlaid with brightfield images (B and D). Images were recorded every minute; time 0 was set as the last time point before anaphase onset. The arrow in B indicates furrow ingression, and a corresponding arrow in D shows the lack of change at the cortex at the same time point after anaphase begins.

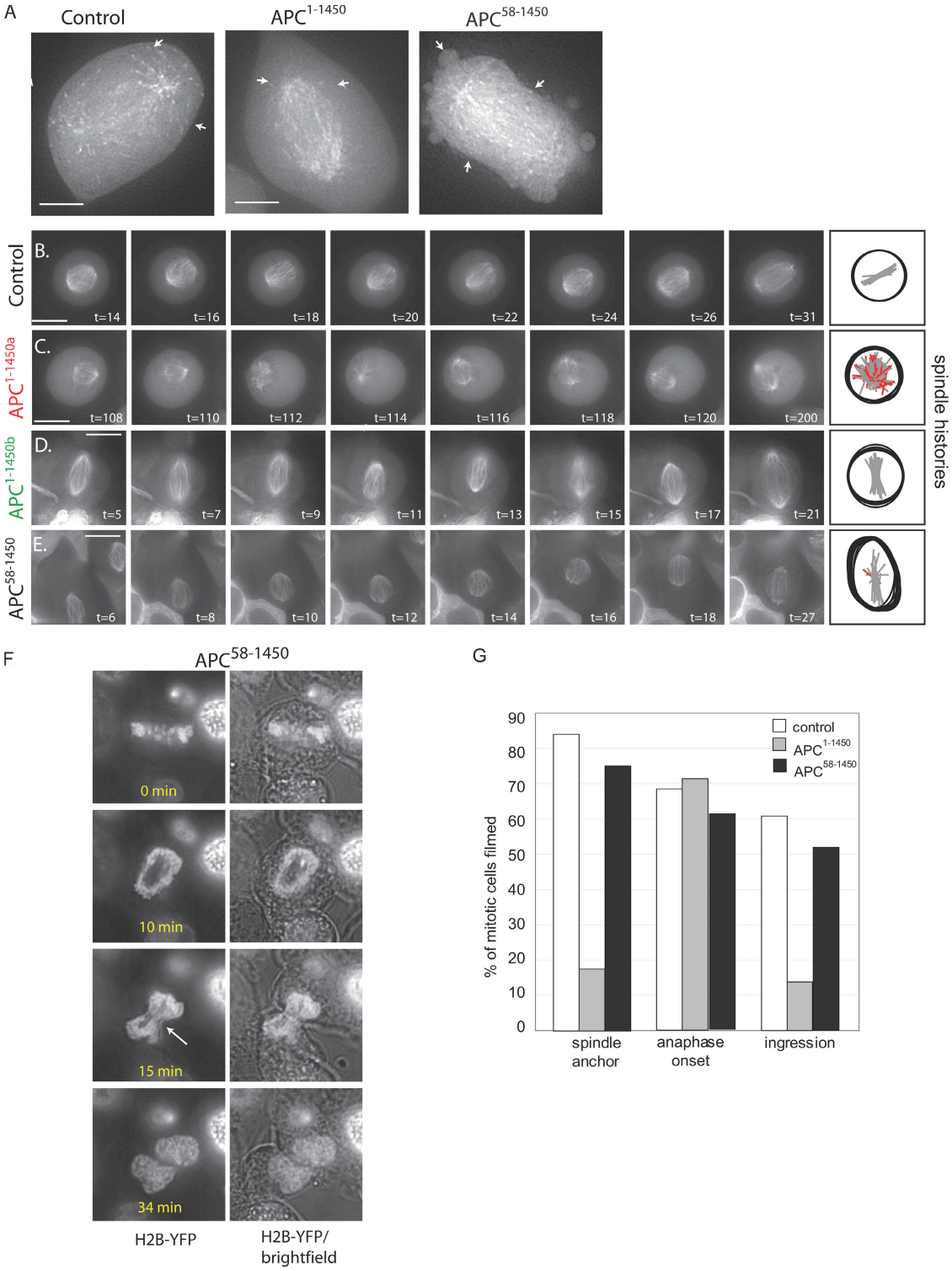

Figure 3. **Spindle anchoring is critical for cytokinesis.** (A) Representative images from videos of the indicated cell lines cotransformed with EB1-GFP (complete videos can be found as Videos 3 and 4, available at http://www.jcb.org/cgi/content/full/jcb.200703186/DC1). Arrows indicate cortical EB1 comets found at the plus ends of microtubules. (B–E) Time points from videos of the indicated cell lines expressing tubulin-GFP are shown (t was set to 0 at the start of filming; complete videos can be found as Videos 5, 6, and 7 corresponding to B, C, and D, respectively). The two examples of cells expressing $APC^{1-1,450}$ include one example of an unsuccessful cytokinesis ($APC^{1-1,450a}$) and one of a successful cytokinesis ($APC^{1-1,450b}$). Spindle histories are presented to the right of each time series. In brief, the cortex of the cell in each video frame was outlined with a circle, and the spindle position was marked with a line. A red line was used to indicate spindles that rotated out of the plane of focus or back into the plane of focus and, thus, could not be represented on the two-dimensional diagram. (F) A stable 293 cell line expressing $APC^{58-1,450}$ was transfected with enhanced GFP–H2B and filmed from metaphase through the completion of cytokinesis. The arrow at the 15-min time point indicates furrow ingression (chromosomes are compressed) in the presence of lagging chromosomes. (G) 68 videos of each cell line expressing either tubulin-GFP, EB1-GFP, or EYFP-H2B were analyzed for spindle anchoring (<15° rotation between 2-min time points), initiation of anaphase (spindle elongation or chromosome separation), and initiation of a cleavage furrow as judged by ingression at the equatorial cortex. Bars, 10 μm.

EB1, or histone 2B were filmed for 1–2 h. In many cases, cells initiated anaphase and formed a cytokinetic furrow during the video. In control cells, we observed the consistent behavior of mitotic spindles documented in videos but more completely depicted in the spindle histories. Spindle histories were created from traces of the cell cortex (circle) and spindle axis (a line) that were derived from each time frame of a video. The tracings were overlaid to provide an entire spindle history (Fig. 3, B–E; right). For example, in control cells during prometaphase and metaphase, spindles moved along their axis but infrequently exhibited large rotational deviations (Fig. 3 B and Video 5, available at http://www.jcb.org/cgi/content/full/jcb.200703186/DC1). These movements decreased as cells entered anaphase and were quickly followed by furrow ingression and cytokinesis. We classified this stable behavior of control spindles as anchored (i.e., $<15°$ of movement between time frames).

Spindles in cells expressing $APC^{1–1,450}$ exhibited two distinct types of behaviors. In >80% of cells filmed, we observed unstable spindle positioning, with spindles more frequently sliding and undergoing large rotations relative to the spindle axis (Fig. 3 C, $APC^{1–1,450a}$; and Video 6, available at http://www.jcb.org/cgi/content/full/jcb.200703186/DC1). The large movements of the spindle were observed equally in metaphase and anaphase cells. In many cases, anaphase was defective with the failed segregation of chromosomes (Video 2) or the reduced elongation of spindles. In <20% of cells, spindles behaved similarly to controls, exhibiting stable spindle anchoring, furrow ingression, and cytokinesis (Fig. 3 D, $APC^{1–1,450b}$; and Video 7). Of the cells that initiated a cytokinetic furrow, there were no consistent changes in the timing of furrow completion between control cells and cells expressing $APC^{1–1,450}$ (Fig. S2 A), arguing that APC mutants do not affect the timing of anaphase. To further examine the relationship between spindle anchoring, anaphase onset, and the initiation of furrow ingression, we collected >100 videos of mitosis for each cell type. We characterized the 68 videos in which we could measure each of the aforementioned parameters (see Materials and methods section Image and statistical analysis). More than 60% of control cells anchored their spindle, entered anaphase, and initiated furrow ingression. In stark contrast, cells expressing $APC^{1–1,450}$ generally failed to anchor their spindles, and, although spindle elongation indicated entry into anaphase, <15% of cells initiated a cytokinetic furrow (Fig. 3 G). A direct tabulation of the relationship between spindle anchoring and furrow initiation more precisely confirmed the trends in Fig. 3 G: regardless of the genotype, we observed a perfect correlation between cells with partially anchored or unanchored spindles and failures to initiate a cytokinetic furrow (Fig. S2 B).

Although we consider the failure to anchor the mitotic spindle the most likely explanation for the failure to induce the cytokinetic furrow, it remains possible that defects in chromosome alignment previously reported in cells expressing $APC^{1–1,450}$ could contribute to inhibition of the cytokinesis (Green and Kaplan, 2003). Indeed, findings in HeLa cells indicate that there is a connection between the rate of lagging chromosomes in anaphase and cytokinetic failure (Shi and King, 2005). To address whether lagging chromosomes or spindle-anchoring defects contribute to cytokinetic failures in APC mutants, we turned to the previously characterized $APC^{58–1,450}$ allele. This allele prevents the oligomerization of mutant and wild-type APC proteins, and spindles exhibit EB1-postive microtubule plus ends near the cell cortex (Fig. 3 A, arrows in $APC^{58–1,450}$). Consistent with stable spindle anchoring, videos of cells expressing $APC^{58–1,450}$ and GFP-tubulin exhibit relatively normal spindle anchoring (Fig. 3 E, spindle history), and >50% of cells have normal cytokinetic ingression (compared with <15% of cells expressing $APC^{1–1,450}$ and >60% for control cells; Fig. 3 G). Despite stable spindle anchoring, cells expressing $APC^{58–1,450}$ have a high rate of misaligned chromosomes in metaphase (>70%) and anaphase cells (>30%), possibly as a result of a decrease in the pause frequency of growing microtubules (Green et al., 2005; and unpublished data). The presence of stably anchored spindles in cells with lagging anaphase chromosomes allowed us to assess whether misaligned chromosomes are sufficient to contribute to a defect in cytokinesis. Despite the obvious presence of chromosomes near the midzone, we did not observe a high rate of bi- or multinucleate cells (Fig. S1 A). Moreover, examples of individual cells expressing H2B-YFP show that chromosomes left behind in the midzone are constricted by the ingressing furrow and clearly do not impede furrow ingression (Fig. 3 F, arrow in the 15-min time point). Thus, $APC^{58–1,450}$ can be considered a separation of function allele (i.e., normal spindle anchoring and cytokinesis but defective chromosome alignment and segregation), and we conclude from this analysis that unanchored spindles but not lagging anaphase chromosomes correlate with a failure to induce cytokinesis in these cells.

Min mice have aberrant mitoses

Although genomic instability has been previously reported in early adenomas in both mice and humans (Shih et al., 2001), our in vitro data suggest that mitotic defects could occur in intestinal epithelium before the appearance of dysplasia or adenomas (i.e., in histologically normal tissue). Specifically, we predicted that changes in microtubule structure and dynamics could result in misoriented mitotic spindles within the gut that could contribute to cytokinetic failure. To test these predictions, we performed a series of analyses of mitoses in the intestinal epithelium of $APC^{Min/+}$ mice (hereafter referred to as *Min* mice) and wild-type littermates at early time points after birth (7–13 wk before the appearance of polyps; Marshman et al., 2002). Importantly, the *Min* allele ($APC^{1–850}$) gives rise to similar mitotic defects as observed for cells expressing $APC^{1–1,450}$. Specifically, we observed that cells expressing $APC^{1–850}$ have an increased incidence of multinucleated cells (fivefold increase), unanchored mitotic spindles (<25% anchored compared with >80% in controls), and a high incidence of anaphase cells that fail to induce a cytokinetic furrow (<20% anchored compared with >60% in controls; Figs. S1 A and S3). We first characterized small intestines of wild-type mice using antibodies against the apical marker ZO-1, the basolateral marker β-catenin to identify cell boundaries, and DAPI to visualize chromosomes. We observed mitotic cells positioned in crypts as expected, and we observed a shift of mitotic chromosomes away from the basement membrane (Fig. S4, A–C; [inset]; available at http://www.jcb.org/cgi/content/full/jcb.200703186/DC1), a position that is consistent with the

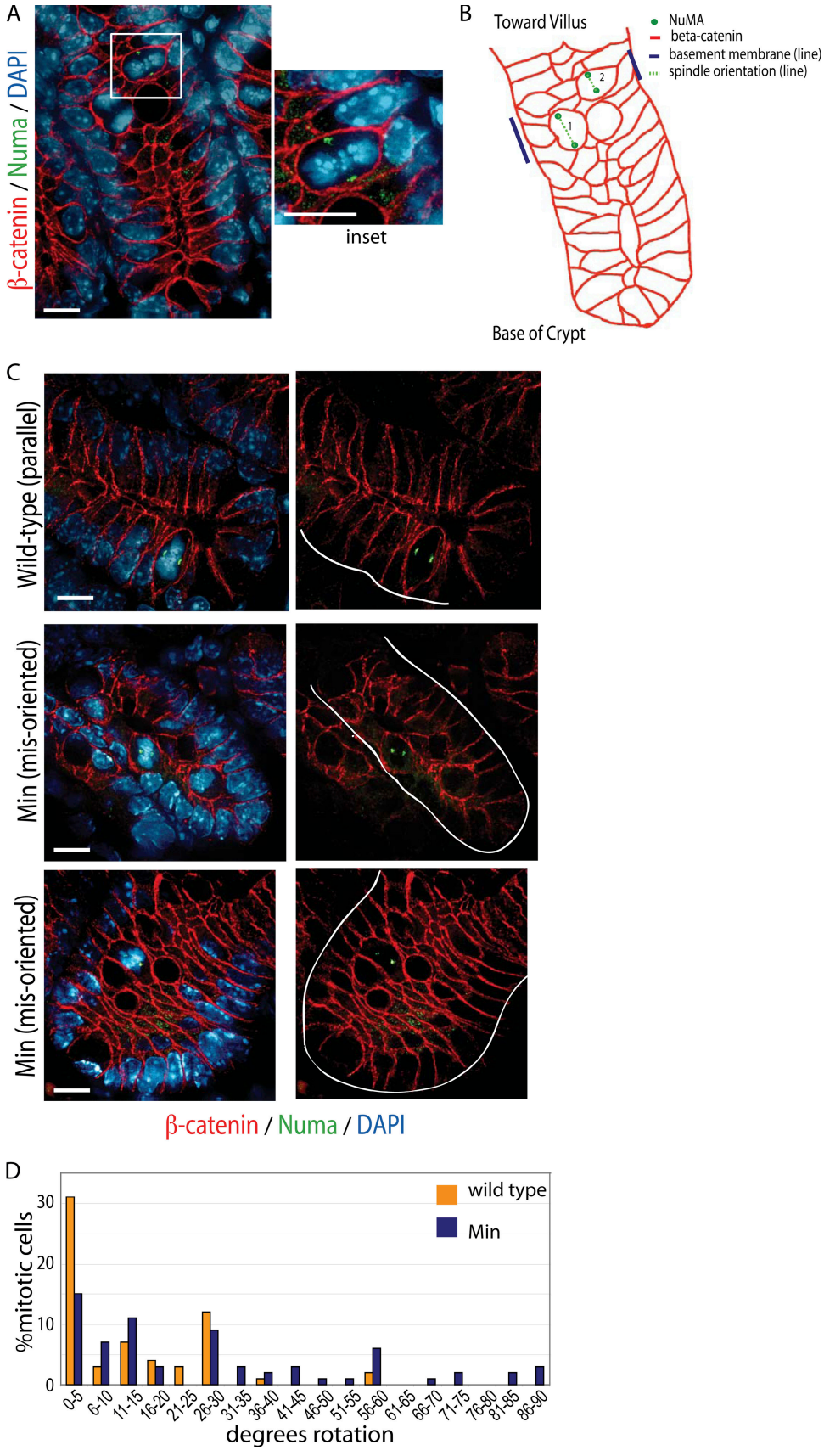

Figure 4. **Min mice have mitotic defects in dividing crypt cells.** (A) Crypts in the small intestine were analyzed using fluorescence microscopy. The cellular boundaries were identified with β-catenin (red), spindles with Numa antibodies (green), and chromosomes with DAPI (blue); a twofold magnification of the boxed area is shown in the inset. (B) Diagram of the cellular organization, position of mitotic cells, and orientation of their spindles for a wild-type mouse.

previous characterization of mitosis in MDCK cell monolayers (Reinsch and Karsenti, 1994).

We next determined the orientation of mitotic spindles in wild-type mice. We used β-catenin staining to visualize the plasma membrane of the cells and a combination of DAPI and Numa (to visualize spindle poles in mitotic cells) staining to orient the spindle with respect to other cells in the crypt and to the basement membrane (Fig. 4 A). We measured the degree of spindle rotation with respect to the basement membrane (Fig. 4 B). In wild-type cells, 95% of metaphase and 85% of anaphase spindles were oriented at an angle of $<30°$. Using this value as a cut-off for proper spindle orientation, we observed a dramatic reduction in properly oriented mitotic spindles in *Min* mice (only 67% of metaphase cells and 53% of anaphase cells had a parallel orientation; $P > 0.001$; see multiple *Min* examples in Fig. 4, C and D). This result is consistent with our in vitro observations that spindles in APC mutant cells fail to properly anchor at the cell cortex (Fig. 3).

Although we cannot clearly view microtubules in these preparations, we observed phenotypes consistent with microtubule defects. We observed that the ratio of the width to length of aligned metaphase chromosomes was increased in *Min* compared with wild-type mice (Fig. S4, D and E) and that chromosomes were often misaligned and failed to reach the metaphase plate (Fig. S4 F). These results are consistent with previous observations made in vitro and attributed to defective spindle microtubules (Green and Kaplan, 2003). Together, defects in chromosome congression, chromosome alignment, and spindle orientation in *Min* mice strongly argue that a truncating mutation in APC induces mitotic defects in vivo by a similar inhibition of microtubule dynamics as demonstrated in vitro (Green et al., 2005).

The mitotic defects we observed in *Min* mice take place in otherwise normal cells. To more directly address the state of these cells with respect to tumor progression, we determined the fate of the full-length (i.e., wild type) APC protein and the levels of β-catenin in *Min* mice intestines. We used a carboxy terminal–specific APC antibody that only recognizes the full-length wild-type APC protein (Fig. S5, A and B; available at http://www.jcb.org/cgi/content/full/jcb.200703186/DC1). In crypts from *Min* mice that exhibit mitotic abnormalities, we observed a characteristic staining of APC at the apical membrane and a basolateral enrichment of β-catenin, patterns that are indistinguishable from crypt cells in wild-type mice (Fig. 5, A and B). By way of comparison, we observed frequent dysplasias in 7-wk-old *Min* mice that are easily distinguishable from the normal organization of the crypts (Fig. 5 C, low magnification image). In contrast to normal crypts, we observed the loss of full-length APC and an increase in the cytoplasmic and nuclear β-catenin signal in every dysplasia analyzed (Fig. 5 D). This analysis shows that cells with a wild-type allele of APC and normal levels of β-catenin exhibit mitotic defects and, therefore, argues that APC mutants compromise mitosis independent of β-catenin deregulation. We further confirmed these conclusions by showing that a single mutant allele of APC does not alter β-catenin levels in vitro (Fig. S5 C) and that expression of stabilized β-catenin in normal 293 cells does not result in cytokinetic failures (Fig. S5, D–F). As expected, we also observed higher levels of multinucleate human colon tumor cells with APC mutations (SW480) but not in colon tumor cell lines with a stabilizing β-catenin mutation (HCT116; Fig. S1 A). We conclude that loss of wild-type APC protein is associated with the earliest stages of dysplasia in *Min* mice and, importantly, that mitotic defects precede the loss of the second allele of APC, β-catenin stabilization, and dysplastic growth.

Tetraploid cells in Min mouse intestines

Our in vitro data establish a link between defects in spindle orientation and failure to induce a cytokinetic furrow. Intriguingly, our observations in *Min* mice suggest that dividing crypt cells have similar spindle orientation defects, raising the possibility that histologically normal crypt cells in *Min* mice are prone to cytokinetic failures. We reasoned that these cytokinetic failures would give rise to tetraploid cells but that these events would be rare. To identify such rare events, we used FISH to determine the copy number of three chromosomes using probes to specific chromosomal regions (APC probe chromosome 8, p53 probe chromosome 11, and tex11 probe X chromosome; see Materials and methods FISH section). We used these probes individually and in pair-wise combinations on intestinal tissues from wild-type and *Min* mice to identify cells with four FISH signals/nucleus.

To ensure accuracy in identifying tetraploid cells, we used several methods. To distinguish between neighboring nuclei, we counterstained samples with DAPI and the membrane dye FM4-64. A representative example of a cross section through a Min mouse intestinal crypt is shown in Fig. 6. The FM4-64 dye was used to make the cell boundaries more apparent in the presentation of optical projections. To unambiguously assign FISH signals to individual nuclei, we analyzed stacks of z-sections that included both FISH signal and the DAPI counterstain. Using these approaches, we could easily identify diploid cells and G2 diploid cells by the close proximity of sister chromatid signals (<1 μm; Fig. 6, D and E). Cells with four well-separated FISH signals were interpreted as being tetraploid, although we cannot rule out a near tetraploid genotype (Fig. 6, C and F). We applied stringent criteria for assigning a tetraploid designation, and, in some cases, we ignored potential tetraploid cells if it was not possible to assign their position in a single nucleus; this may have the effect of underestimating the total number of tetraploid cells. Despite this conservative approach, when a large number of crypts was analyzed, we observed a striking number of cells with four distinct FISH probe signals in *Min* mice (31 cells or 3.1%; Table I; see Discussion). In contrast, there only was one case observed in wild-type mice (0.1%; Table I). Similar trends were observed with all of the FISH probes regardless of whether

The dark blue line indicates the position of the basement membrane, and the dashed green line shows the orientation of the spindle. (C) Small intestine crypts stained as in A from wild-type and *Min* mice (two examples) showing parallel and misoriented mitotic spindles, respectively. (D) Orientation of the mitotic spindle with respect to the basement membrane was determined for >100 mitoses from wild-type and *Min* mice. The rotational angles were separated into 5° increments, and the frequency of spindles in each category was plotted. Bars, 10 μm.

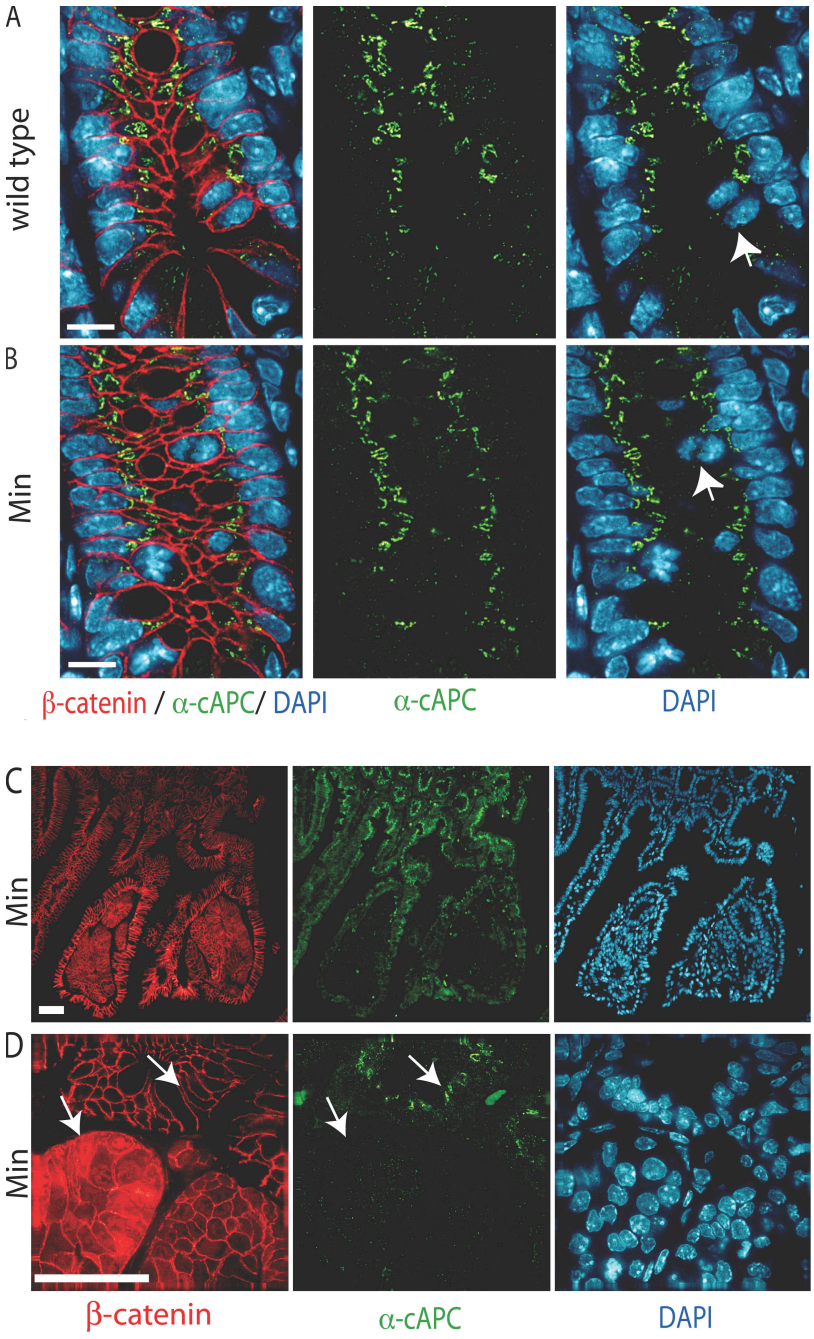

Figure 5. **Mitotic defects occur in histologically normal crypts.** (A and B) Intestinal crypts from wild-type (A) and Min (B) mice were stained with β-catenin (red), an antibody to the C-terminal portion of APC (detects wild-type full-length APC but not truncated APC; see Fig. S5, A and B; available at http://www.jcb.org/cgi/content/full/jcb.200703186/DC1), and DAPI (blue). Arrows indicate the positions of mitotic cells. (C) Low magnification image of dysplastic regions of the intestine stained as in A. (D) High magnification image of dysplastic regions stained as in A. The arrows highlight normal β-catenin levels in cells with wild-type APC and elevated β-catenin levels in cells that have lost wild-type APC. Bars, 10 μm.

they were used individually or in combination, arguing that these cells minimally contain four copies of chromosomes 8, 11, and X (Fig. 6, Table I, and not depicted). These results are consistent with the single mutant allele of APC in *Min* mice promoting the formation of tetraploid cells.

Because the tetraploid cells we observe are isolated events and are predicted to occur only in the epithelial cells of the small intestine, it is not possible to assess their ploidy using more traditional flow cytometry techniques. Therefore, to confirm a tetraploid genotype, we looked for additional characteristics indicative of tetraploid cell formation. Cells harboring a 4N content of DNA are predicted to have larger nuclei than 2N cells. Analysis of DAPI-stained nuclei showed a consistent trend whereby cells with four FISH signals had nearly two times the cross-sectional area as cells believed to be 2N based on their FISH signals (Table II). Second, failures in cytokinesis leave the resulting cell with two centrosomes; subsequent entry into the next cell cycle induces the duplication of centrosomes and the formation of tetrapolar spindles in the next mitosis. We used Numa staining of centrosomes to identify mitotic cells with more than two poles (Fig. 6 G). Importantly, we observed a large number of tetrapolar spindles only in *Min* mice (8/110 in *Min* or 0/105 in wild-type mitotic cells), which is consistent with our in vitro observations of multipolar spindles in cells expressing $APC^{1-1,450}$ (unpublished data). Together, the FISH and cytological features we observed lead us to conclude that tetraploids form in the intestines of Min mice as a result of cytokinetic failures.

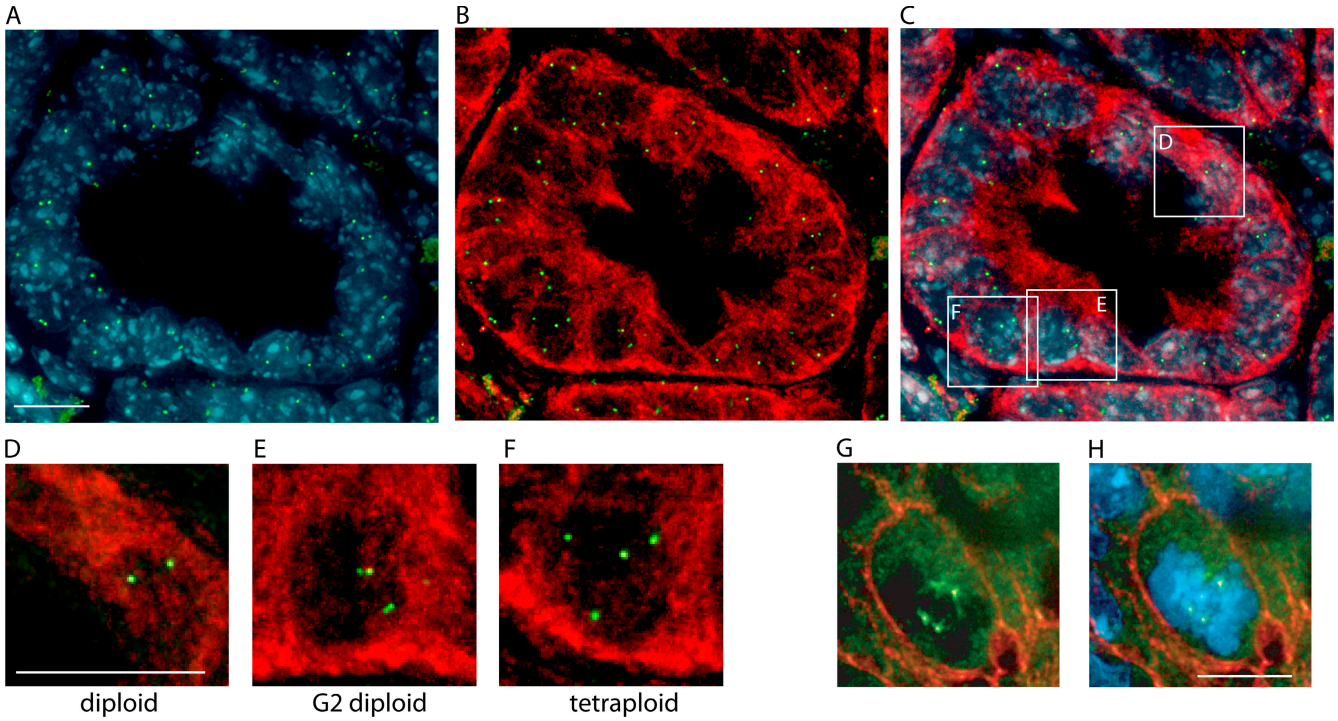

Figure 6. **Min mice have an accumulation of tetraploid cells and exhibit tetraploid cells in the small intestine.** To determine the ploidy of individual cells in the small intestine, FISH was performed using a probe against chromosome 8. (A–F) A micrograph of a representative cross section from an intestinal crypt is shown with FISH (green) and DAPI (blue) counterstain (A), FISH and FM4-64 (red) membrane counterstain (B), or a merge of FISH, DAPI, and FM4-64 staining (C). The areas indicated by the boxes in C are magnified 2.5-fold and provide examples of a normal diploid cell (D), a G2 cell with four FISH signals (E), and a tetraploid cell (F). (G and H) *Min* cells with tetrapolar spindle poles in metaphase were visualized using antibodies to Numa (green). Cell boundaries are demarked by β-catenin staining (red), and chromosomes are stained with DAPI. Bars, 10 μm.

Discussion

Our work shows that clinically relevant mutations in APC act dominantly to inhibit anaphase spindle anchoring, thus resulting in cytokinetic failures in dividing intestinal cells in *Min* mice. This finding implicates a known tumor-initiating mutation in the generation of tetraploid genomes (Fig. 7, red text), a genetic state linked to cancer progression and genomic instability (Fujiwara et al., 2005). The early appearance of tetraploid cells in a mouse model for colorectal cancer argues that these dramatic changes are important for cancer progression.

A major question that remains unanswered pertains to the fate of intestinal cells with tetraploid genomes. Although we expect that tetraploid cells are inherently unstable (minimally because of tetrapolar spindles), the tetraploid model for genomic instability predicts that these cells will give rise to aneuploid cells at the next stage of tumor progression. Unfortunately, it is not trivial to track the fate of a single tetraploid cell in the gut. However, one testable prediction is that dysplasias (Fig. S3) in Min mice will exhibit changes in chromosome ploidy. We find that in contrast to previously reported ploidies of Min tumors (Haigis et al., 2002), dysplasias in Min mice have a notable rate of chromosome gains (4.0% of cells; Table I and see Discussion). This number is likely an underestimate of aneuploidy, as we were not confident assigning FISH signals for chromosome loss events in these regions. This finding supports a model (Fig. 7) whereby APC mutants dominantly induce tetraploid cells in the crypt that resolve to populate dysplastic regions, thus contributing to genomic instability.

Table I. **Tetraploid cells in small intestines**

Mouse	Location	n_{cells}	Two FISH signals/probe	Three FISH signals/probe (%)	Four FISH signals/probe (%)
Min	Crypt	989	565	65 (6.6)	31 (3.1)
Wild type	Crypt	903	457	13 (1.4)	1 (0.1)
Min[a]	Crypt	350	233	32 (9.1)	14 (4.9)
Wild type[a]	Crypt	104	75	5 (4.8)	0 (0)
Min	Dysplasia	218	132	7 (3.2)	4 (1.8)
Min	Villus	153	103	2 (1.3)	3 (2.0)
Wild type	Villus	176	102	0 (0)	0 (0)

[a]Includes crypts with >70% probe hybridization.

Table II. **Size of nuclei in small intestinal cells**

Mouse	*n*	Mean nuclear diameter	SD
		μm^2	
Wild type	50	34.43	10.4
Min, diploid	43	35.36	12.99
Min, 4n	22	51.28	15.66
Min, >2n	28	48.9	14.8
Min, 3n	5	40.15	5.63

$P < 0.00005$, Min diploid versus Min 4n by *t* test.

The mitotic defects we observe in *Min* mice are remarkably similar to those observed in human 293 cells conditionally expressing $APC^{1-1,450}$. Notably, the frequent occurrence of misoriented spindles in *Min* mice is consistent with an in vitro spindle-anchoring defect, and the appearance of tetraploid cells is similar to the formation of binucleate and multinucleate cells in vitro. Together, the collection of parallel phenotypes makes a compelling case that the *Min* mutation compromises microtubule dynamics in vivo, leading to spindle-anchoring defects and the formation of cells with tetraploid genotypes. Therefore, it is important to consider how changes in microtubule behavior that alter cell polarity and chromosome ploidy affect the earliest events in cancer progression.

Do the tetraploid cells we observe in *Min* mice contribute to tumor progression? We observe a remarkably large number of tetraploid cells in crypts: projections based on the number of crypts in the small intestine, the half-life of cells, and their division rate (Marshman et al., 2002) suggest that there are nearly 10^5 tetraploid cells in the small intestine, resulting from one failure in 10^{-2} divisions. Notably, this failure rate is similar to previously published in vitro rates (Lengauer et al., 1997). Obviously, the low number of tumors in *Min* mice (mean = 29 tumors/*Min* mouse) means that not all tetraploid cells give rise to cancer cells. The ability of tetraploid cells to successfully complete another round of mitosis is dependent on their ability to resolve the abnormal configuration of centrosomes and chromosomes. The large number of mitotic cells with tetrapolar spindles in *Min* mice suggests that another round of division is attempted (Fig. 6 D). Such a resolution may give rise to the near diploid or hypotriploid cells observed in intestinal tumors in humans and mice (Cardoso et al., 2006).

Although these results may appear to conflict with previous reports of stable genomes in Min tumors, there are at least two explanations for the differences. The first is that we analyzed tissue earlier in cancer progression than the adenomas reported by Haigis et al. (2002). It is possible that the stabilization of near diploid karyotypes occurs in late stages of tumor formation, when high chromosome number may become a liability to the cancer cell. A second potential factor relates to how the analysis was reported: Haigis et al. (2002) report the total number of FISH signals divided by the total number of cells counted. Although reasonable for gross changes in tumor ploidy, such an approach will fail to identify the low frequency of aneuploid events that we observe in crypt cells or dysplasias. As proof of this point, a similar report of our data gives exactly the same numbers reported by Haigis et al. (2002; unpublished data). The implication is that a constant low frequency of changes in ploidy is ongoing in dysplastic and tumor tissues. Although this rate of ploidy change may be specific for Min mice, its impact on tumor progression remains to be determined. It is interesting to note that Min tumors do not advance

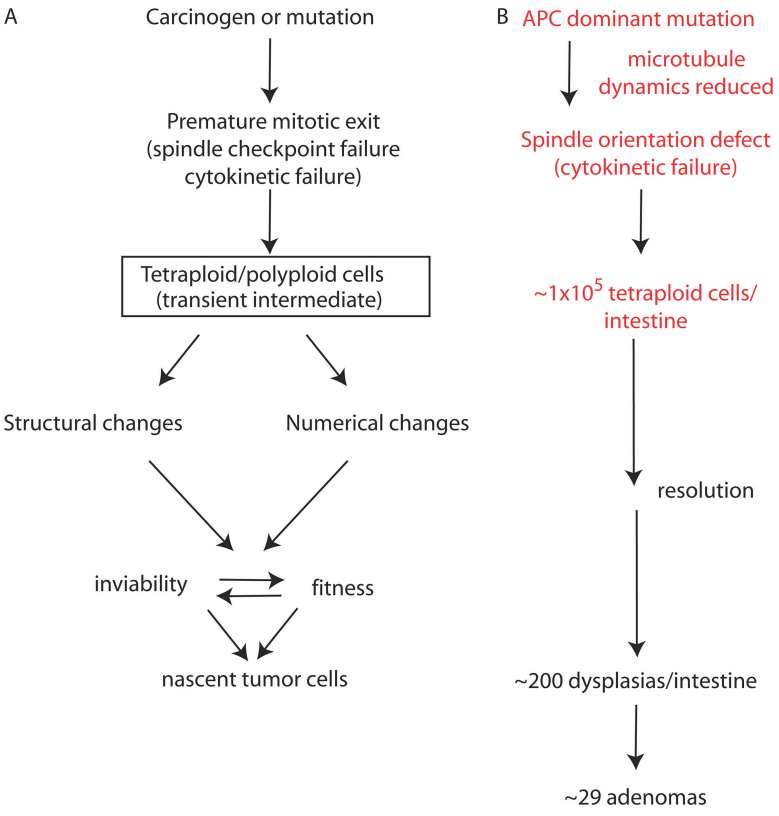

Figure 7. **A model for a transient tetraploid intermediate in cancer progression.** (A) The diagram outlines how genetic lesions or changes caused by environmental stress could, in principle, give rise to mitotic defects and tetraploid cells. Such transient tetraploid cells must resolve their extra centrosomes and large chromosome number to proceed. A strong selection occurs for cells that achieve a balance of structural and numerical changes in chromosomes that favor fitness over inviability and give rise to nascent tumor cells. (B) The data presented in this study are in red, which support the corresponding proposed steps in the model shown in A. The numbers of tetraploid cells and dysplastic regions are reported in this study, whereas the numbers of adenomas are the mean/Min heterozygote reported by Moser et al. (1990).

beyond the adenoma stage, suggesting a potential connection between modifiers of ploidy and disease progression.

Our observations are consistent with the models that posit the evolution of tumor cells (Fig. 7) (Nowell, 1976; Merlo et al., 2006). In this scenario, tetraploid cells in the small intestine form a pool of cells from which aneuploid and/or neoplastic cells sample a variety of genotypes, most of which will fail to give rise to a viable cell and, therefore, avoid the cancer phenotype. These observations argue for a direct path from mitotic defects to cancer and raise important questions as to the molecular and cellular state of these cells at this early stage. It is abundantly clear from our analyses that aneuploidy is a constant and early feature of intestinal epithelium expressing clinically relevant mutations in *APC*. This is the first evidence that a mutation that predisposes patients to colorectal cancer induces chromosomal aneuploidy before any other changes associated with cancer, therefore placing genomic instability in a position to play a causative role in tumor progression.

Materials and methods

Cell lines and antibodies

Regions encoding the indicated fragments of human APC and a 13-myc epitope tag were subcloned for expression, and stable human 293 cell lines were generated as previously described (Green and Kaplan, 2003). Cells were transfected with EB1-GFP (pIK131; provided by J. Tirnauer, University of Connecticut Health Center, Farmington, CT), enhanced GFP–tubulin (pFM258; provided by F. McNally, University of California, Davis, Davis, CA), or enhanced YFP (EYFP)–histone 2B (provided by G. Kops, University Medical Center, Utrecht, Netherlands). Antibodies against c-myc (9E10; Santa Cruz Biotechnology, Inc.), tubulin (Tub2.1 or FITC-conjugated Tub2.1; Sigma-Aldrich), human centromere antigens (anticentromere antibody; Antibodies, Inc.), γ-tubulin (GTU-88; Abcam), or β-catenin (BD Biosciences) were used according to the manufacturers' recommendations. Antibodies against Numa were used at a 1:200 dilution for immunohistochemistry. The c-APC antibody was made by injecting rabbits with a purified recombinant fragment of APC encoding amino acids 2,038–2,843 of the human protein. Specificity of the serum was confirmed by immunoblotting and on APC mutant human tumor cells.

Cell culture

Cells were cultured in DME high glucose medium (Cellgro) supplemented with 10% FCS, 2 mg/ml L-glutamine, 1 mM sodium pyruvate, 200 μg/ml penicillin, and 50 U/ml streptomycin. Cells were maintained at 37°C and 5% CO_2. Plasmid expression vectors for the indicated fusion proteins were transfected into the indicated cell lines using the FuGene 6 reagent (Roche). Cells were treated with ponasterone (Invitrogen) to induce expression of the APC allele 24 h after transfection and were maintained in ponasterone-containing media for 24–48 h before analysis. In the long-term expression experiments, the media was changed every 3–4 d, and fresh ponasterone was added to the media.

Microscopy

Cells were grown on coverslips and processed for immunofluorescence microscopy as previously described (Green and Kaplan, 2003). Fluorescence was collected using an inverted microscope (IX70; Olympus) fitted to an imaging system (DeltaVision RT; Applied Precision). Images were recorded using a 60× NA 1.4 oil immersion lens (for fixed images, live cell imaging, and intestinal sections; Olympus) or a 20× NA 0.75 oil immersion lens (for intestinal sections; Olympus) and a camera (CoolSnap HQ; Roper Scientific). For live cell imaging, cells were grown on 50-mm round coverslips before being transiently transfected with the indicated expression constructs, were allowed to recover for 24 h, and then were induced with ponasterone (as indicated) for 24 h. The coverslip was fitted to a live cell imaging chamber (FCS2; Bioptechs) and maintained at 37°C on the microscope stage. The pH of the media during filming was buffered by the addition of 10 mM Hepes, pH 7.4. An open shutter system was used to rapidly collect 2–4 μm of data at each time point of the video. Deconvolution and image analysis were performed using tools provided in the SoftWorx v 3.5.1 software package (Applied Precision, Inc.).

Mice and immunohistochemistry

Min and wild-type littermate controls were obtained from Jackson ImmunoResearch Laboratories. Mice were housed and maintained according to approved University of California Davis animal protocols. After killing, intestines were removed, fixed as Swiss rolls in 4% formalin overnight, and embedded in paraffin. Paraffin-embedded tissue were cleared and rehydrated according to standard protocols. Tissues were placed in CitraPlus antigen retrieval (Biogenix), heated in a microwave for 4 min, allowed to cool for 1 min, heated for 4 min, cooled for 1 min, and heated for 4 min. Room-temperature slides were rinsed twice in TBS-Tween. Tissues were blocked for 1 h in 50 mM TBS, pH 7.5, 0.1% Tween, 1% BSA, and 2.5% horse and goat serum (Vector Laboratories). Primary antibody was diluted in blocking buffer and incubated for 1 h in a humid chamber and room temperature. Tissue was rinsed twice in blocking buffer. Secondary antibodies were diluted 1:100 in blocking buffer and incubated for 1 h. Tissues were rinsed twice in TBST and once in PBS. Tissues were stained with DAPI for 10 min, rinsed in PBS, and mounted.

FISH

Bacterial artificial chromosomes containing defined portions of the mouse genome were obtained from the BACPAC Resources Center (http://bacpac.chori.org; APC, RP24-73J15; Trp53, RP23-150N14; Tex11, RP24-140K17). FISH was preformed as described previously (Thatcher et al., 2005). The probe mixture consisted of nick-translated labeled probe (digoxigenin-labeled dUTP; Roche) and biotin-labled dUTP (Roche) in LSI/WCP hybridization buffer (Vysis, Inc.) and was denatured on the tissue for 2.5 min at 85°C. When a single biotin-labeled probe was used, the membrane dye FM4-64 (Invitrogen) was incubated at 1:1,000 for 10 min just before adding the DAPI stain and coverslipping the slides.

We noticed variability between discrete regions/crypts, suggesting that the condition of the tissue influences hybridization. To determine hybridization efficiencies of probes using FISH, the following criteria were used: probe signals were required to be within 1.2 μm of in focus DAPI signal, and the total separation allowed between all probe signals was 6 μm. Nuclear diameter was measured at z-section with the largest diameter.

Image and statistical analysis

Analysis of spindle anchoring, anaphase, and furrow initiation parameters were performed on >100 videos for each cell line presented (i.e., control and $APC^{1-1,450}$). Videos in which one parameter could not be determined were discarded (32 videos discarded). Linear regression was used to determine the statistical difference between wild-type and *Min* spindle orientation. A *t* test was used for all other analysis.

Online supplemental material

Fig. S1 is an analysis of binucleate and multinucleate cells in a series of APC mutants and in several colon cancer cell lines. Fig. S2 is an analysis of anaphase timing in wild-type and APC mutant cells, and Fig. S3 presents an expanded analysis of anaphase and spindle histories of cells expressing APC^{1-850}. Fig. S4 provides more detailed views of mitotic cells in intestinal crypts and of the associated mitotic defects found in *Min* mice. In Fig. S5, to validate the carboxy-terminal APC antibody, we provide immunoblot analysis. We also provide evidence that the expression of stabilized β-catenin does not contribute to the accumulation of binucleate and multinucleate cells. Videos 1 and 2 show chromosome behavior in a mitotic control cell (Video 1) and in a mitotic $APC^{1-1,450}$ cell (Video 2). Videos 3 and 4 show EB1-GFP dynamics in control mitotic cells (Video 3) and in $APC^{1-1,450}$ mitotic cells (Video 4). Videos 5 and 6 show mitotic spindle behavior in control cells (Video 5) and in $APC^{1-1,450}$ cells (failed cytokinesis). Video 7 shows mitotic spindle behavior in $APC^{1-1,450}$ cells (successful cytokinesis). Online supplemental material is available at http://www.jcb.org/cgi/content/full/jcb.200703186/DC1.

We would like to thank the following for technical support: Alexander Borowsky, Larry Young, and Lisa Dillard-Temp for help with tissue preparation and histology; Janine LaSalle and Karen Thatcher for assistance with FISH; and Laurel Beckett and Qilu Yu for statistical analysis of mitotic orientation. We thank members of the Kaplan laboratory, the University of California Davis Cytoskeletal Club, and Dr. Bement for important feedback and input on the manuscript.

This work was initiated with funding from a Sidney Kimmel Cancer Foundation grant to K.B. Kaplan and was continued with support from American Cancer Society grants (RSG-02-035-01 and RSG-02-035-05-CCG) and a California Coordinating Committee on Cancer grant to K.B. Kaplan. R.A. Green was funded by a Molecular and Cellular Biology training grant.

Submitted: 28 March 2007
Accepted: 28 August 2007

References

Alsop, G.B., and D. Zhang. 2003. Microtubules are the only structural constituent of the spindle apparatus required for induction of cell cleavage. *J. Cell Biol.* 162:383–390.

Cardoso, J., L. Molenaar, R.X. de Menezes, M. van Leerdam, C. Rosenberg, G. Moslein, J. Sampson, H. Morreau, J.M. Boer, and R. Fodde. 2006. Chromosomal instability in MYH- and APC-mutant adenomatous polyps. *Cancer Res.* 66:2514–2519.

D'Avino, P.P., M.S. Savoian, and D.M. Glover. 2005. Cleavage furrow formation and ingression during animal cytokinesis: a microtubule legacy. *J. Cell Sci.* 118:1549–1558.

Draviam, V.M., I. Shapiro, B. Aldridge, and P.K. Sorger. 2006. Misorientation and reduced stretching of aligned sister kinetochores promote chromosome missegregation in EB1- or APC-depleted cells. *EMBO J.* 25:2814–2827.

Duesberg, P., and R. Li. 2003. Multistep carcinogenesis: a chain reaction of aneuploidizations. *Cell Cycle*. 2:202–210.

Fearnhead, N.S., M.P. Britton, and W.F. Bodmer. 2001. The ABC of APC. *Hum. Mol. Genet.* 10:721–733.

Fodde, R., J. Kuipers, C. Rosenberg, R. Smits, M. Kielman, C. Gaspar, J.H. van Es, C. Breukel, J. Wiegant, R.H. Giles, and H. Clevers. 2001. Mutations in the APC tumour suppressor gene cause chromosomal instability. *Nat. Cell Biol.* 3:433–438.

Fujiwara, T., M. Bandi, M. Nitta, E.V. Ivanova, R.T. Bronson, and D. Pellman. 2005. Cytokinesis failure generating tetraploids promotes tumorigenesis in p53-null cells. *Nature*. 437:1043–1047.

Ganem, N.J., Z. Storchova, and D. Pellman. 2007. Tetraploidy, aneuploidy and cancer. *Curr. Opin. Genet. Dev*. 17:157–162.

Glotzer, M. 2001. Animal cell cytokinesis. *Annu. Rev. Cell Dev. Biol.* 17:351–386.

Green, R.A., and K.B. Kaplan. 2003. Chromosome instability in colorectal tumor cells is associated with defects in microtubule plus-end attachments caused by a dominant mutation in APC. *J. Cell Biol.* 163:949–961.

Green, R.A., R. Wollman, and K.B. Kaplan. 2005. APC and EB1 function together in mitosis to regulate spindle dynamics and chromosome alignment. *Mol. Biol. Cell*. 16:4609–4622.

Haigis, K.M., J.G. Caya, M. Reichelderfer, and W.F. Dove. 2002. Intestinal adenomas can develop with a stable karyotype and stable microsatellites. *Proc. Natl. Acad. Sci. USA*. 99:8927–8931.

Inoue, Y.H., M.S. Savoian, T. Suzuki, E. Mathe, M.T. Yamamoto, and D.M. Glover. 2004. Mutations in orbit/mast reveal that the central spindle is comprised of two microtubule populations, those that initiate cleavage and those that propagate furrow ingression. *J. Cell Biol.* 166:49–60.

Lamlum, H., M. Ilyas, A. Rowan, S. Clark, V. Johnson, J. Bell, I. Frayling, J. Efstathiou, K. Pack, S. Payne, et al. 1999. The type of somatic mutation at APC in familial adenomatous polyposis is determined by the site of the germline mutation: a new facet to Knudson's 'two-hit' hypothesis. *Nat. Med.* 5:1071–1075.

Lengauer, C., K.W. Kinzler, and B. Vogelstein. 1997. Genetic instability in colorectal cancers. *Nature*. 386:623–627.

Marshman, E., C. Booth, and C.S. Potten. 2002. The intestinal epithelial stem cell. *Bioessays*. 24:91–98.

Merlo, L.M., J.W. Pepper, B.J. Reid, and C.C. Maley. 2006. Cancer as an evolutionary and ecological process. *Nat. Rev. Cancer*. 6:924–935.

Morrison, E.E., B.N. Wardleworth, J.M. Askham, A.F. Markham, and D.M. Meredith. 1998. EB1, a protein which interacts with the APC tumour suppressor, is associated with the microtubule cytoskeleton throughout the cell cycle. *Oncogene*. 17:3471–3477.

Moser, A.R., H.C. Pitot, and W.F. Dove. 1990. A dominant mutation that predisposes to multiple intestinal neoplasia in the mouse. *Science*. 247:322–324.

Munemitsu, S., B. Souza, O. Muller, I. Albert, B. Rubinfeld, and P. Polakis. 1994. The APC gene product associates with microtubules in vivo and promotes their assembly in vitro. *Cancer Res.* 54:3676–3681.

Nowell, P.C. 1976. The clonal evolution of tumor cell populations. *Science*. 194:23–26.

Pihan, G.A., J. Wallace, Y. Zhou, and S.J. Doxsey. 2003. Centrosome abnormalities and chromosome instability occur together in pre-invasive carcinomas. *Cancer Res.* 63:1398–1404.

Rappaport, R. 1961. Experiments concerning the cleavage stimulus in sand dollar eggs. *J. Exp. Zool.* 148:81–89.

Reinsch, S., and E. Karsenti. 1994. Orientation of spindle axis and distribution of plasma membrane proteins during cell division in polarized MDCKII cells. *J. Cell Biol.* 126:1509–1526.

Saint, R., and W.G. Somers. 2003. Animal cell division: a fellowship of the double ring? *J. Cell Sci.* 116:4277–4281.

Shi, Q., and R.W. King. 2005. Chromosome nondisjunction yields tetraploid rather than aneuploid cells in human cell lines. *Nature*. 437:1038–1042.

Shih, I.M., W. Zhou, S.N. Goodman, C. Lengauer, K.W. Kinzler, and B. Vogelstein. 2001. Evidence that genetic instability occurs at an early stage of colorectal tumorigenesis. *Cancer Res.* 61:818–822.

Sieber, O.M., I.P. Tomlinson, and H. Lamlum. 2000. The adenomatous polyposis coli (APC) tumour suppressor–genetics, function and disease. *Mol. Med. Today*. 6:462–469.

Smith, K.J., D.B. Levy, P. Maupin, T.D. Pollard, B. Vogelstein, and K.W. Kinzler. 1994. Wild-type but not mutant APC associates with the microtubule cytoskeleton. *Cancer Res.* 54:3672–3675.

Storchova, Z., and D. Pellman. 2004. From polyploidy to aneuploidy, genome instability and cancer. *Nat. Rev. Mol. Cell Biol.* 5:45–54.

Storchova, Z., A. Breneman, J. Cande, J. Dunn, K. Burbank, E. O'Toole, and D. Pellman. 2006. Genome-wide genetic analysis of polyploidy in yeast. *Nature*. 443:541–547.

Su, L.K., M. Burrell, D.E. Hill, J. Gyuris, R. Brent, R. Wiltshire, J. Trent, B. Vogelstein, and K.W. Kinzler. 1995. APC binds to the novel protein EB1. *Cancer Res.* 55:2972–2977.

Thatcher, K.N., S. Peddada, D.H. Yasui, and J.M. Lasalle. 2005. Homologous pairing of 15q11-13 imprinted domains in brain is developmentally regulated but deficient in Rett and autism samples. *Hum. Mol. Genet*. 14:785–797.

Tighe, A., V.L. Johnson, and S.S. Taylor. 2004. Truncating APC mutations have dominant effects on proliferation, spindle checkpoint control, survival and chromosome stability. *J. Cell Sci.* 117:6339–6353.

Wang, Q., Y. Hirohashi, K. Furuuchi, H. Zhao, Q. Liu, H. Zhang, R. Murali, A. Berezov, X. Du, B. Li, and M.I. Greene. 2004. The centrosome in normal and transformed cells. *DNA Cell Biol.* 23:475–489.

Wheatley, S.P., and Y. Wang. 1996. Midzone microtubule bundles are continuously required for cytokinesis in cultured epithelial cells. *J. Cell Biol.* 135:981–989.